Effects of Glycine Substitutions on the Structure and Function of Gramicidin A Channels†

J. B. Jordan,‡,§ S. Shobana,||,▽ O. S. Andersen,|| and J. F. Hinton*,‡

Department of Chemistry and Biochemistry, University of Arkansas, Fayetteville, Arkansas 72701, and Department of Physiology and Biophysics, Weill Medical College of Cornell University, New York, New York 10021

Received August 1, 2006; Revised Manuscript Received September 20, 2006

ABSTRACT: Tryptophan residues often are found at the lipid−aqueous interface region of membrane-spanning proteins, including ion channels, where they are thought to be important determinants of protein structure and function. To better understand how Trp residues modulate the function of membrane-spanning channels, we have examined the effects of Trp replacements on the structure and function of gramicidin A channels. Analogues of gramicidin A in which the Trp residues at positions 9, 11, 13, and 15 were sequentially replaced with Gly were synthesized, and the three-dimensional structure of each analogue was determined using a combination of two-dimensional NMR techniques and distance geometry-simulated annealing structure calculations. Though Trp → Gly substitutions destabilize the $\beta^{6.3}$-helical gA channel structure, it is possible to determine the structure of analogues with Trp → Gly substitutions at positions 11, 13, and 15, but not for the analogue with the Trp → Gly substitution at position 9. The Gly_{11}-, Gly_{13}-, and Gly_{15}-gA analogues form channels that adopt a backbone fold identical to that of native gramicidin A, with only small changes in the side chain conformations of the unsubstituted residues. Single-channel current measurements show that the channel function and lifetime of the analogues are significantly affected by the Trp → Gly replacements. The conductance variations appear to be caused by sequential removal of the Trp dipoles, which alter the ion−dipole interactions that modulate ion movement. The lifetime variations did not appear to follow a clear pattern.

A common feature of membrane-spanning proteins is the presence of amphipathic residues, such as tryptophan and tyrosine, at the aqueous−lipid interface (*1*). This commonality suggests that that these residues play important roles in the structure and function of membrane proteins (*2*), where they may be instrumental in the mechanisms of insertion and anchoring of transmembrane segments into the lipid bilayer (*1*, *3*−*8*). To gain further insight into the importance of Trp residues, we examined how Trp → Gly substitutions modulate the structure and function of gramicidin channels, in which 25% of the amino acids are Trps. Gramicidin A (gA)[1] is a 15-amino acid ion channel-forming polypeptide, with the following sequence (*9*):

Formyl-L-Val-Gly-L-Ala-D-Leu-L-Ala-
D-Val-L-Val-D-Val-L-Trp-D-Leu-L-Trp-
D-Leu-L-Trp-D-Leu-L-Trp-Ethanolamine

gA and many amino acid-substituted gA analogues form bilayer-spanning channels that are antiparallel dimers of two single-stranded, right-handed, $\beta^{6.3}$ helices joined by hydrogen bonds at their N-termini (*10*−*12*). Because of the wealth of information available about gA channel structure and function, the family of linear gramicidins provides an excellent system for elucidating many different aspects of ion channel structure and function (*13*).

Previous studies suggest a role of Trp in insertion and anchoring of the bilayer-spanning channel within the bilayer (*5*, *6*, *8*, *14*−*23*). In addition, though structurally similar (*12*), electrophysiological studies show that the single-channel conductances of channels formed by gA and its two naturally occurring analogues (gB and gC with Phe and Tyr at position 11, respectively) differ, pointing to an additional role of Trp in determining the channels' ion permeability (*24*). The conductance changes rank order with the dipole moment of the residue at position 11 (2.08 D for Trp, 0.0 D for Phe, and 1.4 D for Tyr), suggesting that these residues participate in long-range ion−dipole interactions possibly critical in ion conduction (*15*, *24*). Similar results have been obtained using

† Funding for this project was provided by NSF Grant MCB-9313835 and NIH Grants RR15569-01 and GM21342.

* To whom correspondence should be addressed. E-mail: jhinton@uark.edu. Phone: (479) 575-5143. Fax: (479) 575-4049.

‡ University of Arkansas.

§ Present address: Department of Structural Biology, St. Jude Children's Research Hospital, Memphis, TN 38105.

|| Weill Medical College of Cornell University.

▽ Current address. Corning Incorporated, Science and Technology, Sullivan Park, Corning, New York 14831.

[1] Abbreviations: gA, gramicidin A; Gly_9-gA, Gly_9-gramicidin A; Gly_{11}-gA, Gly_{11}-gramicidin A; Gly_{13}-gA, Gly_{13}-gramicidin A; Gly_{15}-gA, Gly_{15}-gramicidin A; Phe_9-gA, Phe_9-gramicidin A; Phe_{11}-gA, Phe_{11}-gramicidin A; Phe_{13}-gA, Phe_{13}-gramicidin A; Phe_{15}-gA, Phe_{15}-gramicidin A; d_2-TFE, deuterated trifluoroethanol (CF_3CD_2OH); d_{25}-SDS, deuterated sodium dodecyl sulfate; DPhPC, diphytanoylphosphatidylcholine; NMR, nuclear magnetic resonance; DQF-COSY, double-quantum-filtered correlation spectroscopy; TOCSY, total correlation spectroscopy; NOESY, nuclear Overhauser enhancement spectroscopy; DGSA, distance geometry/simulated annealing; For, formyl; Etn, ethanolamine; TAD, torsion angle dynamics.

10.1021/bi061560z CCC: $33.50
Published on Web 11/04/2006

a series of gA analogues with Phe → fluoro-Phe and Trp → fluoro-Trp substitutions (*25*−*30*). However, though the overall channel structure is not affected by Trp → Phe/Tyr replacements at position 11 (*8*, *15*, *24*), structural insights into the consequences of nonaromatic Trp substitutions are limited (*19*).

To assess whether the functional differences caused by Trp substitutions could be due to structural perturbations within the $\beta^{6.3}$-helical framework, we synthesized gA analogues in which the side chain dipoles (and bulk) at the Trp positions are altered and determined the structural consequences, as well as the changes in function. We and others have reported the results of experiments using Trp → Phe substituted analogues of gA (Phe_9-, Phe_{11}-, Phe_{13}-, and Phe_{15}-gA and $Phe_{9,11,13,15}$-gA) which have been shown to form channels having different conductances and lifetimes (*15*, *22*, *31*). In particular, we found that Trp → Phe substitutions exerted little effect on the subunit structure (*8*). Other studies have shown that replacement of Trp_{15} in gramicidin A with Gly (Gly_{15}-gA) results in a significant decrease in single-channel conductance and channel lifetime with only small changes in channel structure (*20*). To complete this study, we now examine gA analogues with Trp → Gly substitutions at positions 9, 11, 13, and 15 (Gly_9-, Gly_{11}-, Gly_{13}-, and Gly_{15}-gA, respectively). Three-dimensional structures could be determined for three of these analogues incorporated into SDS micelles, and their corresponding channel function was assessed electrophysiologically. Here, we compare the structural and functional properties of the analogue channels to those of the native gA channel.

MATERIALS AND METHODS

Gramicidin Synthesis and Purification. The gramicidin A analogues were produced by solid-phase Fmoc peptide synthesis on an Applied Biosystems (Foster City, CA) 431A peptide synthesizer. The amino acid sequence of each analogue was verified using an Applied Biosystems 473A protein sequencer. The purity of each analogue was determined to be >98% using electrospray ionization mass spectrometry (Mass Consortium, San Diego, CA, or University of Arkansas Mass Spectrometry Center). In addition, all analogues used for electrophysiological studies were twice purified using HPLC.

Nondeuterated sodium dodecyl sulfate (SDS) was from PGC Scientifics (Gaithersburg, MD). Deuterated SDS (d_{25}-SDS), deuterium oxide (D_2O), and deuterated trifluoroethanol (CF_3CD_2OH or d_2-TFE) were from Cambridge Isotope Laboratories (Cambridge, MA). d_{25}-SDS was recrystallized twice from 95% ethanol and stored under vacuum for 24 h prior to sample preparation. A 100 mM phosphate buffer solution (pH 6.5) was purchased from PGC Scientifics.

After being incorporated into the SDS micelles, all Trp → Gly substituted analogues were screened for structural homogeneity using previously published methods of Hinton (*32*, *33*). Using nondeuterated SDS, the indole-NH NMR signals were recorded for each analogue. The presence of only three peaks in the indole-NH spectral region (9−11 ppm), one for each indole-NH, indicates the presence of a predominant single-helix species. The presence of more than three signals would indicate the existence of multiple helical conformers. If samples were structurally heterogeneous, the SDS concentration was increased, and the samples were screened again (*32*−*36*). Once a suitable gramicidin:SDS ratio was found, the analogues were incorporated into deuterated SDS micelles at identical concentrations. In our previous study (*20*), Gly_{15}-gA produced a single helical species at the initial 1:50 gramicidin:SDS ratio (5 mM gramicidin and 250 mM SDS). Gly_{13}-gA, however, required a 1:150 ratio (5 mM gramicidin and 750 mM SDS) to adopt a single helical species, and Gly_{11}-gA required an even higher concentration of detergent (∼1:250 gramicidin:SDS). At 5 mM gramicidin, the SDS concentration required to have a single helical species was so high that solution viscosity became a problem, and the gramicidin concentration was decreased to ∼3 mM to allow the use of a lower SDS concentration while maintaining the 1:250 gramicidin:SDS ratio (3 and 750 mM, respectively). Gly_9-gA failed to adopt a single helical species even at the highest useable (900 mM to 1 M) SDS concentrations, rendering the analogue unsuitable for study by NMR methods.

Solutions used for ^1H two-dimensional NMR experiments were prepared in the following manner. A 50 mM solution of the analogue dissolved in d_2-TFE was combined with a 275 mM aqueous d_{25}-SDS solution (90% pH 6.5 buffer and 10% D_2O, v/v). This yielded final concentrations of approximately 5 mM gramicidin and 250 mM d_{25}-SDS (80% pH 6.5 buffer/10% D_2O/10% d_2-TFE). (An 825 mM SDS solution was used for Gly_{13}-gA, yielding final concentrations of 5 mM gramicidin and 750 mM SDS; a 780 mM SDS solution was used for Gly_{11}-gA, yielding final concentrations of 3 mM gramicidin and 750 mM SDS.) The samples were sonicated at low power for 5 min to aid in the incorporation of the gramicidin subunits into the micelles.

NMR Experiments for Structure Determination. NMR experiments were performed using a Bruker Avance 500 MHz NMR spectrometer (Bruker Biospin, Rheinstetten, Germany) equipped with a room-temperature probe. The spectra were recorded at 55 °C to facilitate the measurement of narrow line widths and were acquired in the phase sensitive mode using the States−TPPI method (*37*). Solvent suppression was achieved using transmitter presaturation (*38*). The resonance assignments for all protons were made using DQF-COSY (*39*), TOCSY (*40*), and NOESY (*41*) experiments.

DQF-COSY experiments were acquired using 512 t_1 increments and 8K data points with 128 transients per increment. TOCSY experiments were acquired using 256 t_1 increments and 4K data points with 64 transients per increment. Isotropic mixing was achieved using a mixing time of 75 ms using the MLEV-17 mixing sequence. NOESY experiments were acquired using 512 t_1 increments and 8K data points using 128 transients per increment. The NOESY experiments utilized a 70 ms mixing time, which was found to be within the linear range of the NOE buildup (*12*). All NMR data were processed using the FELIX software available from Accelrys, Inc. (San Diego, CA).

Structure Determination. The three-dimensional structures were determined from the experimentally determined NOE and hydrogen bonding restraints using CNS/ARIA (*28*, *42*) on a home-built Linux cluster. A summary of the restraint information used in the calculations is provided in Table 1. Distance geometry-simulated annealing protocols were used with torsion angle dynamics. In ref *20*, the structures of gramicidin A and its Gly_{15} analogue (PDB entries 1JNO and

Table 1: Constraints Used for Structure Calculations of gA and Its Trp → Gly Analogues

	gA	Gly_{15}-gA	Gly_{13}-gA	Gly_{11}-gA
no. of NOEs				
intramolecular	576	568	586	548
intermolecular	22	22	23	23
per residue	16.9	16.7	17.2	16.1
no. of H bonds				
intramolecular	20	20	20	20
intermolecular	6	6	6	6

1NG8, respectively) were calculated using DSPACE 4.0 (Hare Research Inc., Woodinville, WA). To be consistent, the structures of these two channels were re-determined using newly acquired NMR data and CNS/ARIA. The structures of both gA and Gly_{15}-gA determined by the two different methods were very similar (rmsd of <1.0 Å); small differences were found primarily in the nonaromatic side chains. For calculation of the homodimer structures, each subunit was first modeled as a monomer. NCS (noncrystallographic symmetry) and symmetry restraints were then used with modified DGSA protocols in the calculation of the structure of the symmetric dimers.

Single-Channel Studies. Single-channel conductance measurements were performed in planar lipid bilayers formed from a solution of DPhPC (Avanti Polar Lipids, Alabaster, AL) in *n*-decane (99.9% pure from ChemSampCo, Trenton, NJ) (2−2.5 wt %/volume) at 25 ± 1 °C using the bilayer punch method (*43*). The electrolyte solutions were unbuffered 1.0 M KCl. Aliquots of the Gly analogues dissolved in ethanol were added to the aqueous phases on both sides of the bilayer during stirring. Current signals were recorded using a Dagan 3900 Patch Clamp amplifier (Dagan Corp., Minneapolis, MN), filtered (100−200 Hz) with an eight-pole low-pass Bessel filter, and digitized at 5 times the filter frequency, and the single-channel current transitions were detected using a transition-based algorithm (*43*). Single-channel current transition amplitude histograms were constructed on the basis of the magnitude of the difference in current levels before and after a current transition (*43*) such that the transitions associated with each channel type appear as a single peak in the histograms. The average channel lifetime (τ) was estimated by fitting single-exponential distributions, $N(t) = N(0)\exp(-t/\tau)$, where $N(0)$ is the total number of channels and $N(t)$ denotes the number of channels with a duration longer than time t, to the duration distributions (*44*, *45*).

RESULTS AND DISCUSSION

In this study, we have determined the three-dimensional structures of native gA (*12*) and its Gly_{11}-gA, Gly_{13}-gA, and Gly_{15}-gA (*20*) analogues using solution NMR methods and distance geometry-simulated annealing. For all Trp → Gly substituted analogues, the substitution increased the analogue's conformational flexibility and/or heterogeneity, but as in previous studies (*32*, *33*), most analogues adopted a single conformation as the gramicidin:SDS ratio was increased, thus enabling the determination of their structures by solution NMR. Even at the highest useable SDS concentration (∼900−1000 mM), however, the conformational heterogeneity of Gly_9-gA precluded assignment of the NOESY spectrum, and individual species could not be defined. A similar result has been observed elsewhere with other position 9 substitutions (*19*). For this reason, we focus here on a comparison of the three-dimensional structures and electrophysiological properties of Gly_{11}-, Gly_{13}-, and Gly_{15}-gA with native gA.

Channel Structure. The channel structure of gramicidin has been found to be similar in both SDS micelles and DMPC bilayers (*12*, *46*). In fact, molecular dynamics simulations coupled with solid-state NMR data have shown the backbone structure of both channels to be identical after the structures are allowed to relax (*47*). The Trp_9 side chain, however, appears to be more mobile than those of the other Trp residues, undergoing spontaneous transitions between two states (*47*).

We sought to assess any structural differences caused by Trp → Gly substitution using the three-dimensional structure of each analogue incorporated into SDS micelles. The backbone-NH regions of the NOESY spectra for gA and its Gly_{11}, Gly_{13}, and Gly_{15} analogues exhibit similar characteristics and are shown in Figure 1. On the basis of this information, we calculated minimized average structures of gA and each of the Trp → Gly analogues, as shown in Figure 2. The structures are accompanied by superpositions of the 10 lowest-energy conformers obtained for each analogue in Figure 3. (rmsd statistics for the 10 lowest-energy structures of each analogue are summarized in Table 2.) Figure 4 (panels A−C) shows transverse overlay plots of each analogue with native gramicidin A. To improve the clarity, the formyl and ethanolamine capping groups are excluded. Ethanolamine is known to exhibit extensive conformational flexibility (*12*), and formyl groups, residing at the NH_2-terminal interface, are far removed from the areas of interest and exhibit no structural effects from the substitutions. Results of rmsd analyses of the backbones and side chains of each analogue compared to native gA are summarized in Tables 3 and 4, respectively. These data indicate a high degree of structural homology to native gA, despite the Trp → Gly substitutions.

Effects of Trp → Gly Replacement on Channel Structure. As seen in Figure 4 (panels A−C) and like gA, each analogue studied here forms dimers composed of two single-stranded, right-handed, $\beta^{6.3}$ helices with the monomers being joined by hydrogen bonds at their N-termini.

Gly_{15}-gA exhibits several small deviations (overall rmsd of <1.5 Å) from the structure of native gA resulting from removal of the Trp "anchor" at the channel−solution interface (*18*, *20*). The most significant structural change in Gly_{15}-gA is in the position of the Trp_{11} side chain (Figure 4A), where the indole ring is oriented slightly away from the channel axis, resulting in a small deviation in the position of the Leu_{10} side chain.

The backbone fold is also conserved in Gly_{13}-gA (Figure 4B), though several small side chain deviations from native gramicidin A are evident. Significant changes (rmsd of >1.5 Å) are limited to the D-Leu residues flanking the replaced site (D-Leu_{12} and D-Leu_{14}). Smaller changes (rmsd of ≤1.5 Å) are observed in the ring position of Trp_{15}, with the dipole direction oriented away from the channel lumen. Though small, this reorientation involves a dipole, meaning that the repositioning of Trp_{15} could have some effect on channel function through long-range (electrostatic) ion−side chain interactions (*24*).

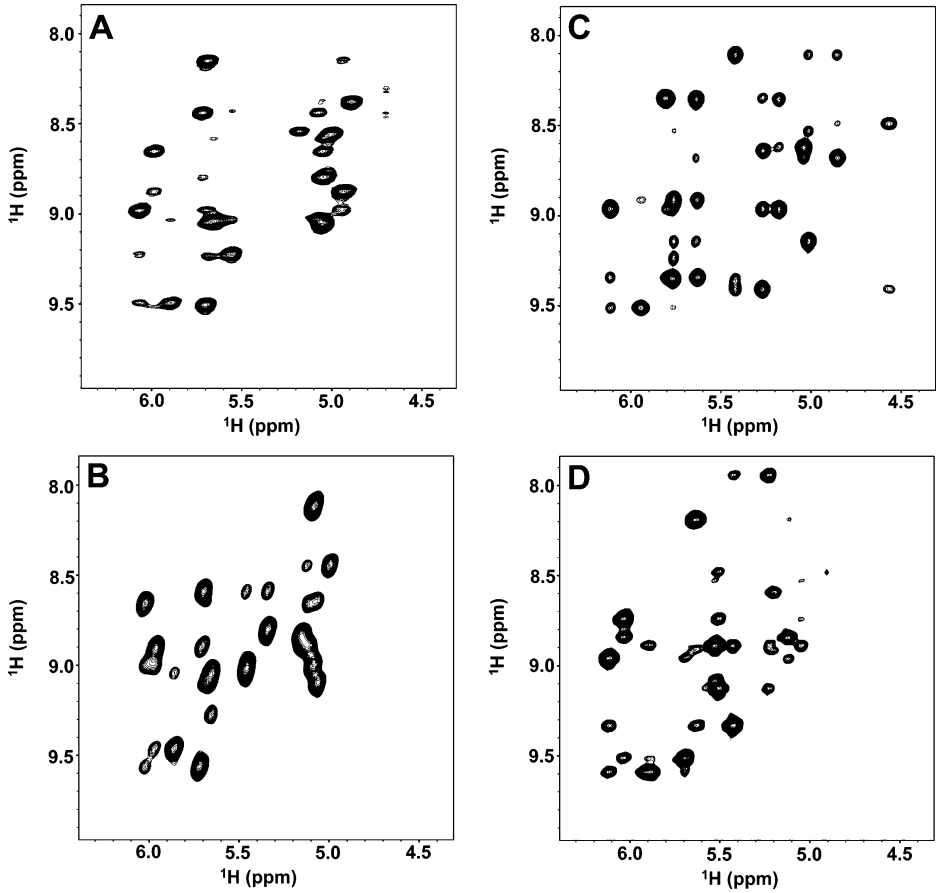

FIGURE 1: Backbone HN regions of the NOESY spectra for gA (A) and its (B) Gly_{15}, (C) Gly_{13}, and (D) Gly_{11} analogues.

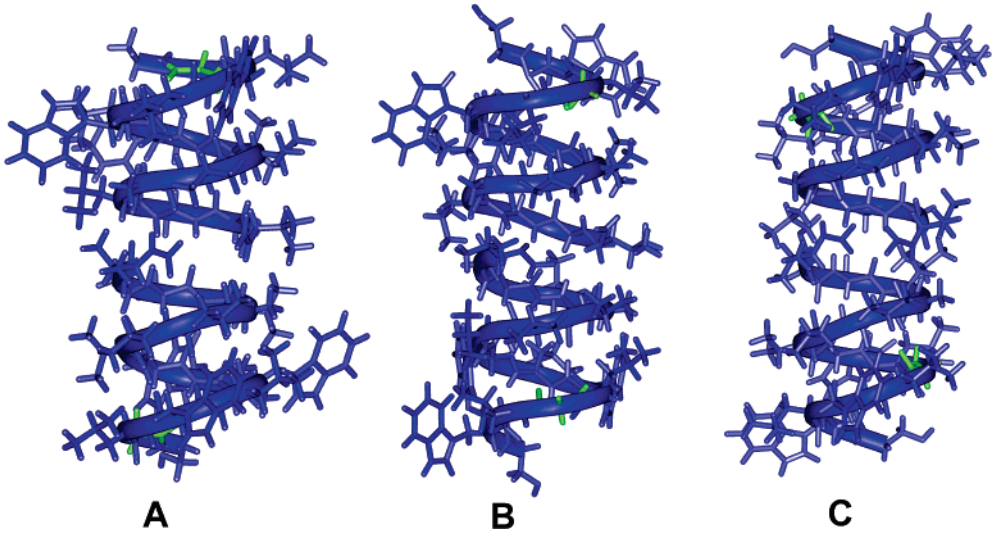

FIGURE 2: Minimized average structures of Gly-substituted gA analogues. Panels A−C show Gly_{15}-gA, Gly_{13}-gA, and Gly_{11}-gA, respectively. The site of substitution is highlighted in green.

Gly_{11}-gA (Figure 4C) exhibits structural deviations smaller than those observed in Gly_{15}- and Gly_{13}-gA. For substitutions involving position 11, i and $i \pm 1$ interactions have the ability to cause changes that can propagate the full length of the helix through long-range interactions ($i \pm 5-7$). Indeed, there are minor (rmsd of <1.5 Å) changes in the positions of the Trp_{15}, Trp_9, and D-Leu_4 side chains. (Though the different D-Leu_4 side chain position could be due to $i - 7$ interactions, it more likely is due to ambiguous chemical shift assignments of the *R* and *S* methylene groups of this residue.) Again, it is possible that the reorientation of Trp_{15} and Trp_9 exerts an influence on channel function due to the movement of Trp dipoles and alterations of side chain−lipid interactions. Overall, the structural effects of Trp → Gly replacements on the gA channel are modest. The small changes observed in these structures maintain a net Trp dipole situated axially with the indole NH group pointed toward the interface region, suggesting that the net dipole orientation in the remaining

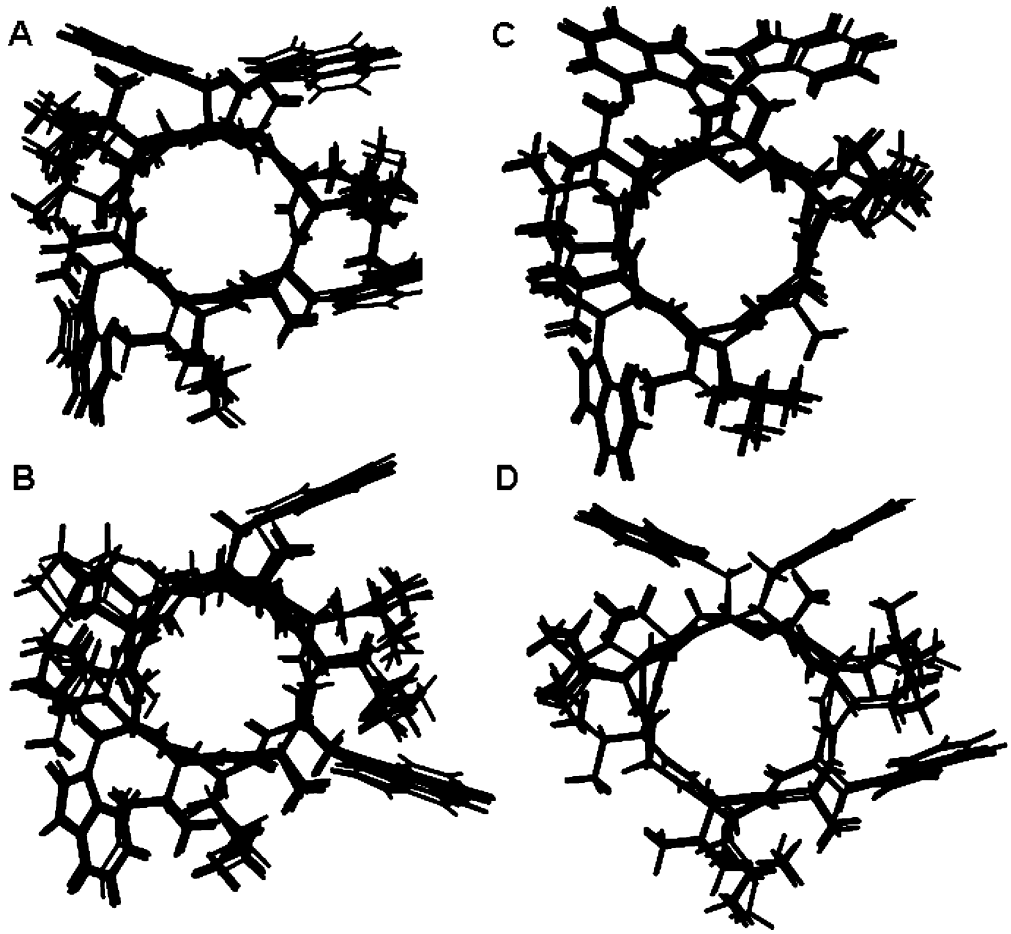

FIGURE 3: Superposition plots of the 10 lowest-energy conformers of (A) gramicidin A, (B) Gly_{15}-gA, (C) Gly_{13}-gA, and (D) Gly_{11}-gA as calculated using ARIA 1.2.

Table 2: Structural Statistics for the 10 Lowest-Energy Structures of gA and Its Trp → Gly Analogues

	gramicidin A	Gly_{15}-gA	Gly_{13}-gA	Gly_{11}-gA
rmsd[a]				
bonds (Å)	0.022	0.023	0.022	0.022
angles (deg)	3.180	3.516	3.285	3.287
impropers (deg)	8.489	8.780	9.054	9.000

[a] All values calculated using ARIA 1.2 (*28*).

Trps is likely to be minimally changed. The more significant structural differences seem to be in the orientation of the D-Leu side chains.

Previous studies (*8*, *32*, *33*) detailing the structural consequences of single-site substitutions can be combined with the results presented here to gain insight into the structural and functional importance of Trp residues in gramicidin channels. Trp residues located at positions 11, 13, and 15 seem to have a modest contribution to the overall conformation of the (bilayer-spanning or micelle-incorporated) gramicidin A channel. Though the tendency to form non-$\beta^{6.3}$-helical conformers becomes stronger as Trp residues closer to the N-terminus are replaced with Gly (or Ala), the predominant conformation is the $\beta^{6.3}$ helix. Only at position 9 does a Trp → Ala, Trp → Gly, or Trp → Phe substitution cause a major shift in the conformational preference, with an almost complete obliteration of the $\beta^{6.3}$-helical conformer (*8*, *33*). Thus, whereas drastic substitutions at Trp positions 11, 13, and 15 have little effect on the overall channel structure, even subtle substitutions at position 9 seem to completely alter gramicidin's ability to fold into $\beta^{6.3}$ helices. This qualitative difference could be due to the more buried (*12*) and less water accessible (*48*) position of Trp_9. Indeed, molecular dynamics simulations show that Trp_9 is more mobile than the other Trps (*47*).

In addition to direct effects of Trp substitutions, indirect effects may also be observed. Replacement of the D-Leu "spacer" residues in the gA sequence (D-Leu_{10}, $-_{12}$, and $-_{14}$) imposes significant changes on the gramicidin channel structure (*49*). The bulky Leu residues seemingly lock the Trp rings in positions optimal for ion transport and channel stabilization (*50*). Taken together with the consistent positioning of the Trp rings in gA and its Phe (Phe_{15}, Phe_{13}, and Phe_{11}) and Gly (Gly_{15}, Gly_{13}, and Gly_{11}) analogues, it appears that the D-Leu residues at positions 10, 12, and 14 affect the ability of gA to form a stable helical species by modulating the orientation and dynamics of the Trp rings. These influences may also be affected by the lipid bilayer environment. However, previous studies have shown that in identical environments, even minor changes in the primary sequence at any one of the spacer residues have a profound effect on the ability of the peptide to adopt a single helical species (*49*).

Effects of Trp → Gly Substitution on Single-Channel Conductance. As expected from the conserved $\beta^{6.3}$-helical structure, Trp → Gly substituted gA analogues form ion-conducting channels (at least in the case of Gly_{11}-, Gly_{13}-, and Gly_{15}-gA; technical difficulties have prevented the

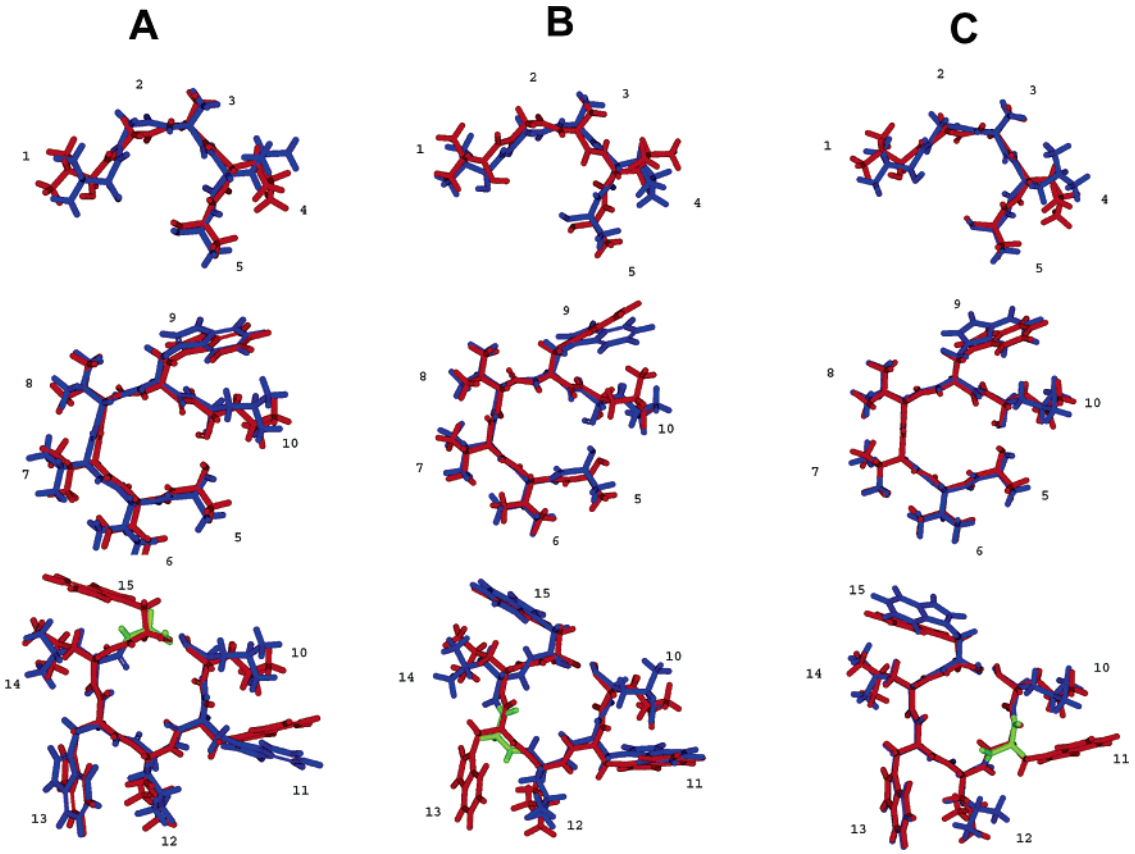

FIGURE 4: Transverse sliced overlay plots of Gly analogues with native gramicidin A. Panels A−C show Gly_{15}-gA, Gly_{13}-gA, and Gly_{11}-gA, respectively, colored blue overlaid on native gA colored red. The site of replacement in the Gly analogues is highlighted in green.

Table 3: Residue-By-Residue Backbone Root-Mean-Square Deviations[a] (angstroms) for Each Gly Analogue Relative to gA

residue	Gly_{15}-gA	Gly_{13}-gA	Gly_{11}-gA
1	1.00	0.94	0.91
2	0.83	0.77	0.53
3	0.43	1.09	0.45
4	0.89	0.83	0.70
5	0.65	1.01	0.52
6	0.44	0.21	0.34
7	0.54	0.27	0.09
8	0.31	0.38	0.16
9	0.45	0.33	0.24
10	0.54	0.73	0.31
11	0.35	0.62	0.38
12	0.79	0.84	0.33
13	0.50	0.64	0.38
14	0.98	1.07	0.26
15	0.75	0.46	0.39

[a] All rmsd values calculated using Crystallography and NMR System (*42*).

Table 4: Residue-By-Residue Side Chain Root-Mean-Square Deviations (angstroms) for Each Gly Analogue Relative to gA[a]

residue	Gly_{15}-gA	Gly_{13}-gA	Gly_{11}-gA
1	1.20	1.20	1.40
2	—[b]	—[b]	—[b]
3	0.79	1.05	0.76
4	1.07	1.48	2.20
5	1.00	1.26	0.74
6	0.59	0.11	0.31
7	0.66	0.20	0.19
8	0.56	0.63	0.41
9	0.57	0.64	1.10
10	2.22	1.56	1.30
11	1.87	0.58	—
12	1.51	1.67	1.90
13	0.34	—	0.46
14	1.94	2.07	0.50
15	—	1.57	1.10

[a] The sites of substitution are omitted due to the presence of different residues at these locations. All rmsd values calculated using Crystallography and NMR System (*42*). [b] Glycine residues with no side chain.

recording of Gly_9-gA channel activity). To compare the effects of the Trp → Gly substitutions on channel function, the functional characteristics of each analogue were determined using single-channel electrophysiology. As expected, channel function is affected to a greater extent by replacements closer to the N-terminus of the channel (*15*, *18*, *32*, *33*, *51*) in a rank order that is the opposite of that for the substitution-induced changes in the analogue's propensity to fold as $\beta^{6.3}$-helical subunits.

Figure 5 shows a single-channel current trace, a single-channel current transition amplitude, and lifetime histograms for channels formed by Gly_{13}-gA; Figure 6 shows similar results for Gly_{11}-gA. The results are summarized in Table 5. In each case, the analogue forms a single type of conducting channels, which can be seen in the single major peak in the current transition amplitude histograms (panel B) and the single-exponential lifetime distribution (panel C). In addition to the results for Gly_{13}- and Gly_{11}-gA channels, Table 5 summarizes the results for channels formed by gA and Gly_{15}-gA and, for comparison, channels formed by Phe_{15}-, Phe_{13}-, and Phe_{11}-gA. For all analogues, the current−voltage characteristics in 1.0 M KCl are approximately linear (Figure 7).

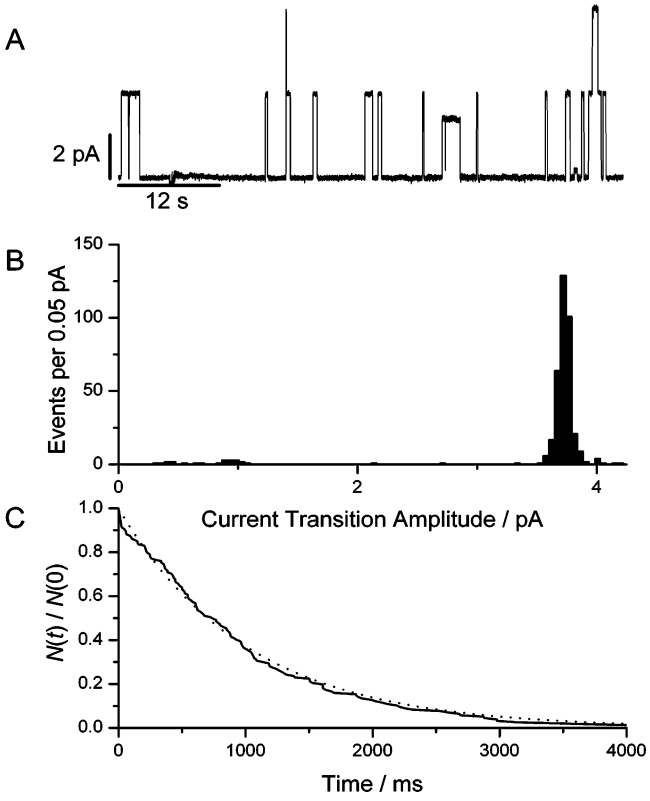

FIGURE 5: Characterization of Gly_{13}-gA channel function. (A) Single-channel current trace. (B) Current transition amplitude histogram, plotted as the magnitude of the difference in current level just before and just after a current transition. (C) Single-channel lifetime distribution (plotted as a normalized survivor plot) and single-exponential fit (···), with 1.0 M KCl at 200 mV.

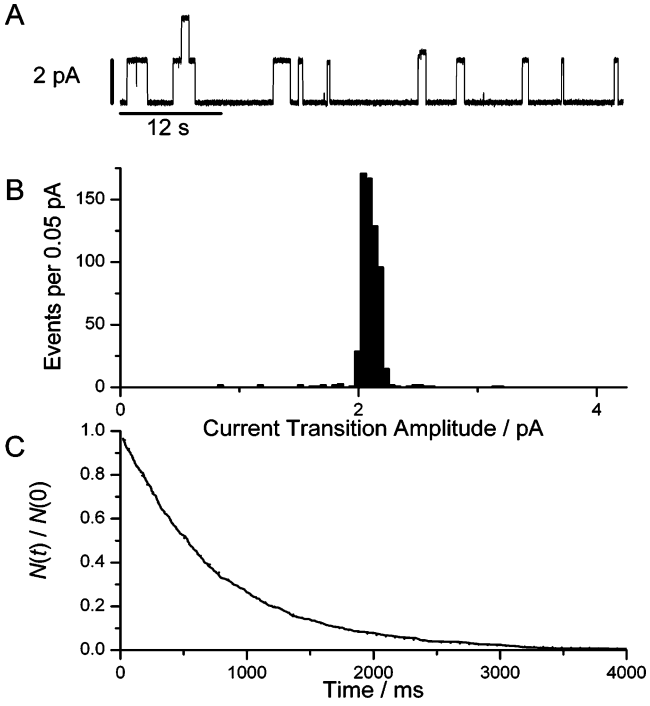

FIGURE 6: Characterization of Gly_{11}-gA channel function. (A) Single-channel current trace. (B) Current transition amplitude histogram, plotted as the magnitude of the difference in current level just before and just after a current transition. (C) Single-channel lifetime distribution (plotted as a normalized survivor plot) and a single-exponential fit (···), with 1.0 M KCl at 200 mV.

Table 5: Single-Channel Conductances and Average Lifetimes of Trp-Substituted gA Analogues in 1.0 M KCl at 200 mV and 25 ± 1 °C

	conductance[a] (pS)	lifetime[b] (ms)
gA	27.5 ± 0.3	740
Gly_{15}-gA	17.3 ± 0.4	210
Gly_{13}-gA	19.0 ± 0.8	1010
Gly_{11}-gA	10.9 ± 0.7	750
Phe_{15}-gA	22.2 ± 0.8	1200
Phe_{13}-gA	24.5 ± 0.6	1140
Phe_{11}-gA	19.3 ± 0.7	1920

[a] Mean ± standard deviation. [b] The uncertainly in the lifetimes is ~10%.

The electrophysiological results using Trp → Gly substitutions largely mirror those obtained with Trp → Phe substitutions (see also ref *15*). Substitution of the Trp side chains with side chains with smaller dipole moments results in lower conductance relative to that of the native gA channels. Substitutions at positions 15 and 13 have nearly the same effect, with the conductance values of Gly_{15}- or Phe_{15}-gA channels being slightly lower than those of the Gly_{13}- or Phe_{13}-gA channels. These results are similar to those obtained with Na^+ as the permeant ion in the Trp to Phe substituted channels, where the conductance of Phe_{13}-gA channels is also higher than that of Phe_{15}-gA channels (*15*). Substitutions at position 11 have much more pronounced effects, whether the substituted residue is a Gly or a Phe. At all positions that were tested, the relative conductance variations are greater with the Trp → Gly substituted channels than with the Trp → Phe substituted channels.

Ion movement through gA channels involves a series of sequential steps: ion entry, ion translocation through the channel, and ion exit. Trp substitutions can alter all of these steps through long-range ion−dipole interactions between the permeating ion and the indole side chain, as well as short-range interactions between the permeating ion and the peptide backbone lining the pore. The gramicidin channel possesses two binding sites for monovalent cations, one in each subunit ~10 Å from the channel center (*52*), which are encompassed by residues 10−15 (*53*−*56*). Ion binding is believed to involve the carbonyl oxygen atoms of these residues (*57*, *58*), with additional stabilization conferred by ion−dipole interactions with the Trp side chains, as suggested by the results with Trp → Phe substituted (*15*, *59*) and fluoro-Trp gA analogues (*18*, *19*, *30*). Like Gly substitutions, Phe substitutions cause only minor perturbations in channel structure (*8*), suggesting that the conductance changes primarily reflect the sequential loss of Trp dipoles, each of which promotes cation entry, binding, and permeation (*12*, *15*, *59*). The stronger effects of the Trp → Gly substitutions, as compared to Trp → Phe substitutions (Table 5), suggest that short-range ion−peptide backbone interactions also may be involved. In either case, whether Trp → Gly or Trp → Phe substitutions, the stronger effect of Trp_{11} substitutions is likely to reflect the fact that the more buried (N-terminal) Trp residues will have an increasingly important effect on the central barrier to ion translocation through the channels (*30*, *59*).

Effects of Trp → Gly Replacement on Channel Lifetime. In contrast to the conductance changes caused by Trp → Gly substitutions, the single-channel lifetimes (Table 5) do not follow any obvious trend. Importantly, the results observed with channels formed by Trp → Gly analogues

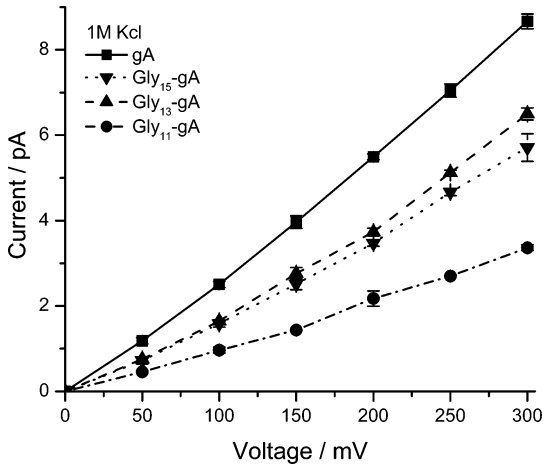

FIGURE 7: Current−voltage relations for channels formed by gA (■), Gly_{15}-gA (▼), Gly_{13}-gA (▲), and Gly_{11}-gA (●), with 1.0 M KCl.

differ from those observed with channels formed by Trp → Phe analogues. This divergence suggests that alteration of channel lifetimes cannot result solely from the removal of the Trp residues; the identity of the substituted residue is important as well. Given the complex variation of lifetimes with multiple Trp → Phe substitutions (*15*), we refrain from analyzing the lifetime variations further.

Conclusions. Trp → Gly substitutions at positions 15, 13, and 11 progressively destabilize the $\beta^{6.3}$-helical gA channel fold, with little effect on the $\beta^{6.3}$-helical structure, once formed. Though the substitutions have little effect on channel structure, they cause large changes in channel function, providing further support for the importance of the amphipathic Trp side chains for gA channel structure and function. When comparing the changes observed with channels formed by Trp → Gly analogues to those observed with channels formed by Trp → Phe analogues, we conclude that the changes in function cannot be due solely to the removal of the bulky, dipolar Trp side chains. Given the much more pronounced changes in ion permeability with Trp → Gly versus Trp → Phe substitutions, we tentatively conclude that changes in ion−peptide backbone interactions, caused by the increased backbone flexibility conferred by the Gly residues and altered side chain−side chain interactions caused by the removal of the bulky Trp residues, are important for directing gA channel function.

REFERENCES

1. Schiffer, M., Chang, C. H., and Stevens, F. J. (1992) The functions of tryptophan residues in membrane proteins, *Protein Eng. 5*, 213−4.
2. Wallace, B. A. (2000) Common structural features in gramicidin and other ion channels, *BioEssays 22*, 227−34.
3. Killian, J. A., Timmermans, J. W., Keur, S., and de Kruijff, B. (1985) The tryptophans of gramicidin are essential for the lipid structure modulating effect of the peptide, *Biochim. Biophys. Acta 820*, 154−6.
4. Henderson, R., Baldwin, J. M., Ceska, T. A., Zemlin, F., Beckmann, E., and Downing, K. H. (1990) Model for the structure of bacteriorhodopsin based on high-resolution electron cryomicroscopy, *J. Mol. Biol. 213*, 899−929.
5. Durkin, J. T., Providence, L. L., Koeppe, R. E., II, and Andersen, O. S. (1992) Formation of non-β6.3-helical gramicidin channels between sequence-substituted gramicidin analogues, *Biophys. J. 62*, 145−59.
6. Hu, W., Lee, K. C., and Cross, T. A. (1993) Tryptophans in membrane proteins: Indole ring orientations and functional implications in the gramicidin channel, *Biochemistry 32*, 7035−47.
7. Wallace, B. A., and Janes, R. W. (1999) Tryptophans in membrane proteins. X-ray crystallographic analyses, *Adv. Exp. Med. Biol. 467*, 789−99.
8. Jordan, J. B., Easton, P. L., and Hinton, J. F. (2005) Effects of phenylalanine substitutions in gramicidin A on the kinetics of channel formation in vesicles and channel structure in SDS micelles, *Biophys. J. 88*, 224−34.
9. Sarges, R., and Witkop, B. (1965) Gramicidin A. V. The Structure of Valine- and Isoleucine-Gramicidin A, *J. Am. Chem. Soc. 87*, 2011−20.
10. Arseniev, A. S., Barsukov, I. L., Bystrov, V. F., Lomize, A. L., and Ovchinnikov, Yu. A. (1985) ^{1}H-NMR study of gramicidin A transmembrane ion channel. Head-to-head right-handed, single-stranded helices, *FEBS Lett. 186*, 168−74.
11. Russell, E. W., Weiss, L. B., Navetta, F. I., Koeppe, R. E., II, and Andersen, O. S. (1986) Single-channel studies on linear gramicidins with altered amino acid side chains. Effects of altering the polarity of the side chain at position 1 in gramicidin A, *Biophys. J. 49*, 673−86.
12. Townsley, L. E., Tucker, W. A., Sham, S., and Hinton, J. F. (2001) Structures of gramicidins A, B, and C incorporated into sodium dodecyl sulfate micelles, *Biochemistry 40*, 11676−86.
13. Andersen, O. S., Koeppe, R. E., II, and Roux, B. (2006) Gramicidin Channels: Versatile Tools, in *Biological Membrane Ion Channels: Dynamics, Structure, and Applications* (Chung, S.-H., Andersen, O. S., and Krishnamurthy, V. V., Eds.) Springer, New York.
14. O'Connell, A. M., Koeppe, R. E., II, and Andersen, O. S. (1990) Kinetics of gramicidin channel formation in lipid bilayers: Transmembrane monomer association, *Science 250*, 1256−9.
15. Becker, M. D., Greathouse, D. V., Koeppe, R. E., II, and Andersen, O. S. (1991) Amino acid sequence modulation of gramicidin channel function: Effects of tryptophan-to-phenylalanine substitutions on the single-channel conductance and duration, *Biochemistry 30*, 8830−9.
16. Hu, W., and Cross, T. A. (1995) Tryptophan hydrogen bonding and electric dipole moments: Functional roles in the gramicidin channel and implications for membrane proteins, *Biochemistry 34*, 14147−55.
17. Yau, W. M., Wimley, W. C., Gawrisch, K., and White, S. H. (1998) The preference of tryptophan for membrane interfaces, *Biochemistry 37*, 14713−8.
18. Koeppe, R. E., II, Killian, J. A., Greathouse, D. V., and Andersen, O. S. (1998) Tryptophan anchors in transmembrane proteins, *Biol. Skr.−K. Dan. Vidensk. Selsk. 49*, 93098.
19. Cotten, M., Tian, D., Busath, D. D., Shirts, R. B., and Cross, T. A. (1999) Modulating dipoles for structure-function correlations in the gramicidin A channel, *Biochemistry 38*, 9185−97.
20. Sham, S. S., Shobana, S., Townsley, L. E., Jordan, J. B., Fernandez, J. Q., Andersen, O. S., Greathouse, D. V., and Hinton, J. F. (2003) The structure, cation binding, transport, and conductance of Gly15-gramicidin A incorporated into SDS micelles and PC/PG vesicles, *Biochemistry 42*, 1401−9.
21. Separovic, F., Hayamizu, K., Smith, R., and Cornell, B. A. (1991) C-13 chemical shift tensor of L-tryptophan and its application to polypeptide structure determination, *Chem. Phys. Lett. 181*, 157−62.
22. Separovic, F., Gehrmann, J., Milne, T., Cornell, B. A., Lin, S. Y., and Smith, R. (1994) Sodium ion binding in the gramicidin A channel. Solid-state NMR studies of the tryptophan residues, *Biophys. J. 67*, 1495−500.
23. Separovic, F., Ashida, J., Woolf, T. B., Smith, R., and Terao, T. (1999) Determination of chemical shielding tensor of an indole carbon and application to tryptophan orientation of a membrane peptide, *Chem. Phys. Lett. 303*, 493−8.
24. Mazet, J. L., Andersen, O. S., and Koeppe, R. E., II (1984) Single-channel studies on linear gramicidins with altered amino acid sequences. A comparison of phenylalanine, tryptophane, and tyrosine substitutions at positions 1 and 11, *Biophys. J. 45*, 263−76.
25. Koeppe, R. E., II, Mazet, J. L., and Andersen, O. S. (1990) Distinction between dipolar and inductive effects in modulating the conductance of gramicidin channels, *Biochemistry 29*, 512−20.

26. Andersen, O. S., Greathouse, D. V., Providence, L. L., Becker, M. D., and Koeppe, R. E., II (1998) Importance of Tryptophan Dipoles for Protein Function: 5-Fluorination of Tryptophans in Gramicidin A Channels, *J. Am. Chem. Soc. 120*, 5142−6.
27. Busath, D. D., Thulin, C. D., Hendershot, R. W., Phillips, L. R., Maughan, P., Cole, C. D., Bingham, N. C., Morrison, S., Baird, L. C., Hendershot, R. J., Cotten, M., and Cross, T. A. (1998) Noncontact dipole effects on channel permeation. I. Experiments with (5F-indole)Trp13 gramicidin A channels, *Biophys. J. 75*, 2830−44.
28. Linge, J. P., Habeck, M., Rieping, W., and Nilges, M. (2003) ARIA: Automated NOE assignment and NMR structure calculation, *Bioinformatics 19*, 315−6.
29. Thompson, N., Thompson, G., Cole, C. D., Cotten, M., Cross, T. A., and Busath, D. D. (2001) Noncontact dipole effects on channel permeation. IV. Kinetic model of 5F-Trp(13) gramicidin A currents, *Biophys. J. 81*, 1245−54.
30. Cole, C. D., Frost, A. S., Thompson, N., Cotten, M., Cross, T. A., and Busath, D. D. (2002) Noncontact dipole effects on channel permeation. VI. 5F- and 6F-Trp gramicidin channel currents, *Biophys. J. 83*, 1974−86.
31. Heitz, F., Gavach, C., Spach, G., and Trudelle, Y. (1986) Analysis of the ion transfer through the channel of 9,11,13,15-phenylalanylgramicidin A, *Biophys. Chem. 24*, 143−8.
32. Hinton, J. F., Washburn-McCain, A. M., Snow, A., and Douglas, J. (1997) Effects of alanine and glycine substitution for tryptophan on the heterogeneity of gramicidin A analogs in micelles, *J. Magn. Reson. 124*, 132−9.
33. Hinton, J. F., and Washburn, A. M. (1995) Species heterogeneity of Gly-11 gramicidin A incorporated into sodium dodecyl sulfate micelles, *Biophys. J. 69*, 435−8.
34. Colnago, L. A., Valentine, K. G., and Opella, S. J. (1987) Dynamics of fd coat protein in the bacteriophage, *Biochemistry 26*, 847−54.
35. Leo, G. C., Colnago, L. A., Valentine, K. G., and Opella, S. J. (1987) Dynamics of fd coat protein in lipid bilayers, *Biochemistry 26*, 854−62.
36. Killian, J. A., Trouard, T. P., Greathouse, D. V., Chupin, V., and Lindblom, G. (1994) A general method for the preparation of mixed micelles of hydrophobic peptides and sodium dodecyl sulphate, *FEBS Lett. 348*, 161−5.
37. States, D., Haberkorn, R., and Ruben, D. (1982) A two-dimensional nuclear Overhauser experiment with pure absorption phase in four quadrants, *J. Magn. Reson. 48*, 286−92.
38. Hoult, D. (1976) Solvent peak saturation with single phase and quadrature fourier transformation, *J. Magn. Reson. 21*, 337.
39. Piantini, U., Sorensen, O. W., and Ernst, R. R. (1982) Multiple quantum filters for elucidating NMR coupling networks, *J. Am. Chem. Soc. 114*, 10663−5.
40. Braunschweiler, L., and Ernst, R. R. (1983) Coherence transfer by isotropic mixing: Application to proton correlation spectroscopy, *J. Magn. Reson. 53*, 521−8.
41. Jeener, J., Meier, B. H., Bachmann, P., and Ernst, R. R. (1979) Investigation of exchange process by two-dimensional NMR spectroscopy, *J. Chem. Phys. 71*, 4546−53.
42. Brunger, A. T., Adams, P. D., Clore, G. M., DeLano, W. L., Gros, P., Grosse-Kunstleve, R. W., Jiang, J. S., Kuszewski, J., Nilges, M., Pannu, N. S., Read, R. J., Rice, L. M., Simonson, T., and Warren, G. L. (1998) Crystallography & NMR system: A new software suite for macromolecular structure determination, *Acta Crystallogr. D54* (Part 5), 905−21.
43. Andersen, O. S. (1983) Ion movement through gramicidin A channels. Single-channel measurements at very high potentials, *Biophys. J. 41*, 119−33.
44. Sawyer, D. B., Koeppe, R. E., II, and Andersen, O. S. (1989) Induction of conductance heterogeneity in gramicidin channels, *Biochemistry 28*, 6571−83.
45. Durkin, J. T., Koeppe, R. E., II, and Andersen, O. S. (1990) Energetics of gramicidin hybrid channel formation as a test for structural equivalence. Side-chain substitutions in the native sequence, *J. Mol. Biol. 211*, 221−34.
46. Cross, T. A. (1997) Solid-state nuclear magnetic resonance characterization of gramicidin channel structure, *Methods Enzymol. 289*, 672−96.
47. Allen, T. W., Andersen, O. S., and Roux, B. (2003) Structure of gramicidin a in a lipid bilayer environment determined using molecular dynamics simulations and solid-state NMR data, *J. Am. Chem. Soc. 125*, 9868−77.
48. Maruyama, T., and Takeuchi, H. (1997) Water accessibility to the tryptophan indole N-H sites of gramicidin A transmembrane channel: Detection of positional shifts of tryptophans 11 and 13 along the channel axis upon cation binding, *Biochemistry 36*, 10993−1001.
49. Hinton, J. F., Jordan, J. B., and Horne, E. (2002) Molecular structure heterogeneity of gramicidin analogs incorporated into SDS micelles: A NMR study, *J. Mol. Struct. 602*−*603*, 245−56.
50. Jude, A. R., Greathouse, D. V., Koeppe, R. E., II, Providence, L. L., and Andersen, O. S. (1999) Modulation of gramicidin channel structure and function by the aliphatic "spacer" residues 10, 12, and 14 between the tryptophans, *Biochemistry 38*, 1030−9.
51. Tucker, W. A., Fletcher, T. G., and Hinton, J. F. (1993) Three-dimensional structure of gramicidin in SDS micelles, *Biophys. J. 64*, 299.
52. Olah, G. A., Huang, H. W., Liu, W. H., and Wu, Y. L. (1991) Location of ion-binding sites in the gramicidin channel by X-ray diffraction, *J. Mol. Biol. 218*, 847−58.
53. Prasad, K. U., Trapane, T. L., Busath, D., Szabo, G., and Urry, D. W. (1982) Synthesis and characterization of 1-(13) C-D X Leu12,14 gramicidin A, *Int. J. Pept. Protein Res. 19*, 162−71.
54. Hinton, J. F., Buster, D. C., Easton, P., and Privett, T. (1988) Metal ion NMR study of cation transport through the gramicidin channel, *Prog. Clin. Biol. Res. 273*, 331−6.
55. Urry, D. W., Jing, N., Trapane, T. L., Luan, C. H., and Waller, M. (1988) Ion interactions with the gramicidin A transmembrane channel: Cesium-133 and calcium-43 NMR studies, *Curr. Top. Membr. Transp. 33*, 51−90.
56. Hinton, J. F. (1996) Cation-binding location and hydrogen-exchange sites for gramicidin in SDS micelles using NOESY NMR, *J. Magn. Reson., Ser. B 112*, 26−31.
57. Urry, D. W. (1984) Molecular structure of the gramicidin transmembrane channel: Utilization of carbon-13 nuclear magnetic resonance, ultraviolet absorption, circular dichrosim, and infrared spectroscopies, *NATO ASI Ser. C 139*, 487−510.
58. Smith, R., Thomas, D. E., Atkins, A. R., Separovic, F., and Cornell, B. A. (1990) Solid-state ^{13}C-NMR studies of the effects of sodium ions on the gramicidin A ion channel, *Biochim. Biophys. Acta 1026*, 161−6.
59. Becker, M. D., Koeppe, R. E., II, and Andersen, O. S. (1992) Amino acid substitutions and ion channel function. Model-dependent conclusions, *Biophys. J. 62*, 25−7.

BI061560Z